PHYSICAL REVIEW E **81**, 045401(R) (2010)

# Effects of plasma wave packets and local pump depletion in stimulated Raman scattering

B. J. Winjum,[1] J. E. Fahlen,[2] F. S. Tsung,[1] and W. B. Mori[1,2]
[1]*Department of Physics and Astronomy, University of California, Los Angeles, California 90095, USA*
[2]*Department of Electrical Engineering, University of California, Los Angeles, California 90095, USA*
(Received 24 August 2009; published 12 April 2010)

Through one-dimensional and two-dimensional (2D) particle-in-cell simulations of stimulated Raman scattering (SRS), we show that nonlinear plasma wave packets that are created during SRS and convect through the system after saturation can have a dramatic effect on the recurrence of the instability. The recurrence rate is shown to depend on the propagation speed and frequency content of these packets. Furthermore, SRS can be driven to higher amplitudes via backscattered light traveling between packets. In 2D, the influence of the plasma wave packets is also seen, but the average reflectivity is substantially less due to geometric effects and transverse localization of the packets.

DOI: 10.1103/PhysRevE.81.045401 PACS number(s): 52.38.Bv, 52.35.Fp, 52.35.Mw, 52.65.−y

Stimulated Raman scattering (SRS), the decay of a light wave into a scattered light wave and an electron plasma wave, involves fundamental wave-wave and wave-particle interactions. It has been extensively studied in regimes relevant to inertial confinement fusion (ICF), where it can reduce the drive energy and generate hot electrons that potentially preheat the target. Computer simulations of SRS have shown that the instability consists of subpicosecond bursts and involves several nonlinear kinetic processes such as nonlinear frequency shifts [1], sidebands [2], beam acoustic modes [3], beam acoustic decay [4], vortex-merging [5], and kinetic inflation [6]. These simulations have focused on the threshold and saturation mechanisms of SRS in the hope that they could then be incorporated into theoretical models. However, the bursty nature of SRS in time and space with finite-width packets of plasma and light waves traveling between both stable and unstable regions of plasma has not been well characterized.

Simulations show that SRS plasma waves are spatially localized [3] and convect as plasma wave packets after saturation [2,4]. Previous work has largely ignored the effects of packet behavior on SRS reflectivity. Strozzi *et al.* showed convecting plasma packets but did not study their effect on SRS behavior [4]. Fahlen *et al.* [7] recently showed how nonlinear plasma wave packets propagate and damp, in particular showing how newly trapped particles etch the rear edge of the plasma wave packet. In this Rapid Communication we show via one-dimensional (1D) and two-dimensional (2D) particle-in-cell (PIC) simulations using the fully explicit electromagnetic PIC code OSIRIS [8] how nonlinear plasma wave packets affect the recurrence and reflectivity of SRS. Following SRS growth and saturation, the resulting plasma wave packets convect through the plasma. Even though the initial saturation has occurred, the frequency-shifted packet continues to reflect the incident laser with a recurrence rate that depends on the nonlinear frequency shift of the packet. This continued scattering locally depletes the incoming laser energy, but as the packet is etched and the effects of pump depletion decrease, there can be renewed packet growth. After the packet has moved a sufficient distance into the plasma, a new burst of SRS will grow, creating a new packet in the region left behind. Thus, the recurrence rate also depends on the packet speed. Finally, new bursts of SRS can interact with scattered light coming from packets that are farther into the plasma, provided the interaction length is long enough to permit several packets to coexist. 2D simulations of a single diffraction-limited speckle also show these effects.

The 1D (2D) simulations use 8192 ($8192\times512$) cells with 512 (256) particles per cell to simulate plasmas of length 30, 60, and 100 $\mu$m (100 $\mu\text{m}\times14$ $\mu$m). The ions were fixed to focus purely on SRS; mobile ion simulations have been performed and do not affect the conclusions shown. The electrons had a temperature and density of $T_e=3$ keV and $n_e=0.128n_{cr}$ ($k\lambda_D=0.30$ for backward SRS). The driving laser had a wavelength $\lambda_0=0.351$ $\mu$m and intensity $I_0=1.5\times10^{15}-2.8\times10^{15}$ W/cm$^2$ in 1D, while the laser in 2D was focused from $I_0=1.5\times10^{15}$ W/cm$^2$ at the simulation edge to $I_0=2.5\times10^{15}$ W/cm$^2$ at center (focus) with a spot size of 2.6 $\mu$m ($8\lambda_0$). The laser propagates along $\hat{x}$ and is polarized in $\hat{z}$. The simulations had absorbing (in $\hat{x}$) and periodic (in $\hat{y}$ and $\hat{z}$) boundaries for the fields and thermal-bath boundaries for the particles.

As several different lengths, $L$, and driving laser intensities, $I_0$, were simulated, $L$ and $I_0$ will also be noted in the discussion. These parameters are similar to those used in Refs. [1–4,6,9], but $T_e$ is more NIF-relevant (3 versus 0.7–1.5 keV) and $k\lambda_D$ is intermediate between 0.26 [1,2,6] and 0.34 [3,4,9]. Simulations spanning all of these parameters have been performed with similar results; the results shown here were chosen as clear examples.

Figure 1(a) shows the enveloped temporal evolution of the reflected light at the incident boundary (left) and the spatiotemporal evolution of the backscattered light (middle) and plasma waves (right) in the 1D, 30 $\mu$m simulation. Three packets of SRS-generated plasma waves grow and convect over the total simulation, but the reflectivity shows many more than three bursts due to continued reflection from frequency-shifted plasma wave packets. During SRS growth and saturation, a plasma packet grows in amplitude and traps particles, resulting in a negative frequency shift in qualitative agreement with the theory of Morales and O'Neil [10]. A detailed calculation of the frequency shift of a nonlinear plasma wave in SRS has been the subject of recent study [11–13], but a comparison with simulation results is left for

 

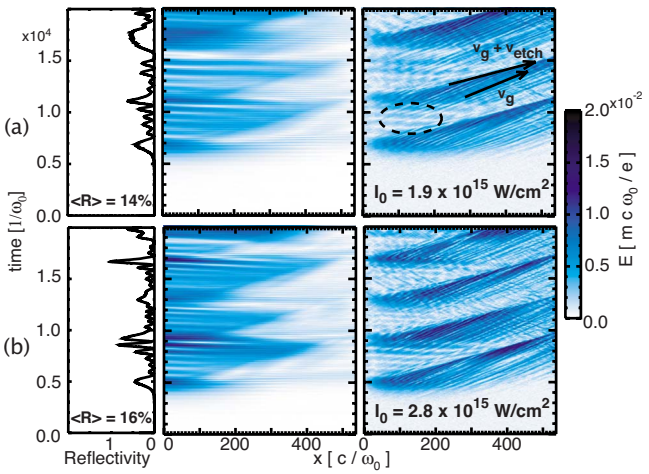


FIG. 1. (Color online) Time vs reflectivity (left) and time vs space of the backward-propagating light (middle) and $E_x$ field (right). The simulation parameters are equivalent with the exception of driving laser intensity $I_0$ as noted.

the future. The peak amplitude is a factor of two less than the Coffey limit [14] and saturation is due to detuning from the nonlinear frequency shift. After saturation, these packets of frequency down-shifted plasma waves convect forward. As they convect, new laser energy enters the system. The frequency matching condition for SRS growth, $\omega_0=\omega_1+\omega_2$, where $\omega_{0,1,2}$ are the laser, scattered, and plasma wave frequencies, respectively, can be maintained if $\omega_1$ shifts positively for the negative shift in $\omega_2$. The frequency-matching condition is then satisfied by $\omega_0=(\omega_1+\Delta\omega)+(\omega_2-\Delta\omega)$.

As the frequency up-shifted light moves outside the packet, however, the frequency-matching condition can no longer be satisfied. The beat of the scattered light wave with the incident laser nonresonantly drives SRS in the background plasma left behind the packet with $\omega_0=(\omega_1+\Delta\omega)+\omega_{NR}$, where the dielectric $\epsilon(k,\omega_{NR})\neq 0$. Like a simple harmonic oscillator driven off-resonance, the nonresonant drive produces a low frequency beat pattern with maxima separated in time at $\tau=2\pi/\Delta\omega$. This beat pattern can be seen in areas behind the packets, for example, in Fig. 1(a) in the circled region, and additionally in the reflected light. The plasma wave initially grows secularly as pump energy is transferred to the reflected light and plasma waves, but the detuning causes the growth to saturate and energy to be transferred from the reflected light and plasma waves back to the pump. This effect manifests itself as the high frequency recurrence in the reflected and transmitted light. We measure $\Delta\omega/\omega_0\simeq 0.008$, giving $\tau\simeq 800\omega_0^{-1}$ in good correspondence with the burst times of the reflectivity in Fig. 1(a), left.

Reflectivity bursts also come from new SRS growth. These stronger bursts occur less frequently and can be seen in Fig. 1(a) (left and middle) as the three large peaks at $\omega_0 t\simeq 7000$, 11 500, and 17 000. As packets convect forward, new SRS bursts grow in the region of plasma left behind once there is a sufficiently large region for gain. Their recurrence therefore depends on how quickly packets leave, which is determined by the speed of the rear side of the packet. As was shown by Fahlen *et al.* [7], the packet convection speed is faster than the group velocity, $v_g$, of the SRS plasma wave because packets are continually etched by resonant particles traveling at the phase velocity, $v_\phi > v_g$. As shown by the arrows in Fig. 1(a), the rear side of the packet has a speed $v_{packet}=v_g+v_{etch}$, where $v_{etch}$ is the packet's etching speed. Here we measure $v_{packet}=1.4v_{th}$, slightly lower than that predicted by [7]. However, strict agreement is not expected as the plasma waves here are continuously driven outside the packet by recurring SRS in the convecting packets, a process affecting trapped particle motion behind the packet and thereby the etching rate.

To show that $v_{packet}$ affects the recurrence rate, Fig. 1(b) shows a simulation with the same plasma parameters but a higher driving laser intensity (2.8 vs $1.9\times 10^{15}$ W/cm$^2$). Since the convective gain length is shorter, the packets do not have to travel as far before a sufficient length is available for convective growth of a new burst. The packet speeds in Figs. 1(a) and 1(b) are nearly the same, despite the larger plasma wave amplitudes, since the etching rate is only weakly dependent on the amplitude for these conditions. With a similar packet speed but a shorter distance to travel, the time for new bursts is shorter and consequently the recurrence rate of new bursts is faster. Furthermore, the recurrence rate of high-frequency bursts from scattering off convecting packets is slightly faster as well since the higher amplitude plasma waves have a slightly larger frequency shift ($\Delta\omega/\omega_0\simeq 0.01$ and $\tau\simeq 600$). The effect of $v_{packet}$ can also be clearly seen in backscattered light for both cases. Figure 1 makes clear that the backscattered light originates deeper in the plasma for the low intensity case. It also shows that the packet's rear edge, moving at $v_{packet}$, acts like a barrier, continually reflecting and locally pump-depleting the incoming laser. The time-averaged reflectivity is 14% and 16%, respectively, indicating that 50% higher intensity increases the reflectivity only slightly.

Since each packet leaves the interaction length before the next packet is well established, the recurrence of new bursts in both simulations is fairly periodic. When the interaction length is long enough for packets to stay in the system during the growth of new bursts, SRS behavior becomes more complex. Figure 2 shows the SRS activity for a simulation with identical parameters as Fig. 1(a) except for a doubled interaction length (60 vs 30 $\mu$m). With a longer length, the total time-averaged reflectivity is larger (34%) for several reasons. First, the reflectivity bursts from each packet's growth are higher, even for the first burst. Even though the saturated plasma waves have comparable amplitude for both lengths at approximately half the Coffey limit, they are excited over a larger region in the longer simulation, leading to more backscattered light and a larger burst of reflectivity at the edge. Pump depletion plays a role in the saturation for this case. The bursts of reflectivity from the first convecting packet have the same periodicity for both simulations as well, since the frequency shifts are comparable.

Second, new packet growth does not occur solely in the region left behind by packets. For the longer plasma of Fig. 2(a), the packet can nearly etch away before it propagates across the system, allowing the pump to reach further into the plasma. The second plasma "packet" grows at ($x\omega_0/c\simeq 600$ and $\omega_0 t\simeq 8000$), giving the second major

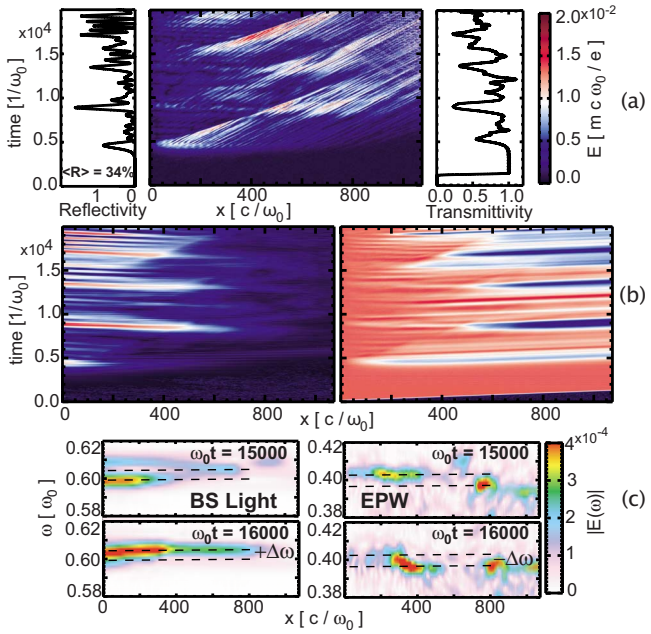


FIG. 2. (Color online) (a) Reflectivity vs time (left), transmittivity vs time (right), and time vs space of the $E_x$ field (middle) for $L=60$ $\mu$m and $I_0=1.9\times10^{15}$ W/cm$^2$. (b) Spatiotemporal evolution of backward (left) and forward (right) propagating light for the same simulation. (c) Spatial-frequency content of the transverse (left) and longitudinal (right) $E$ fields at two times during packet convection obtained by a windowed FFT.

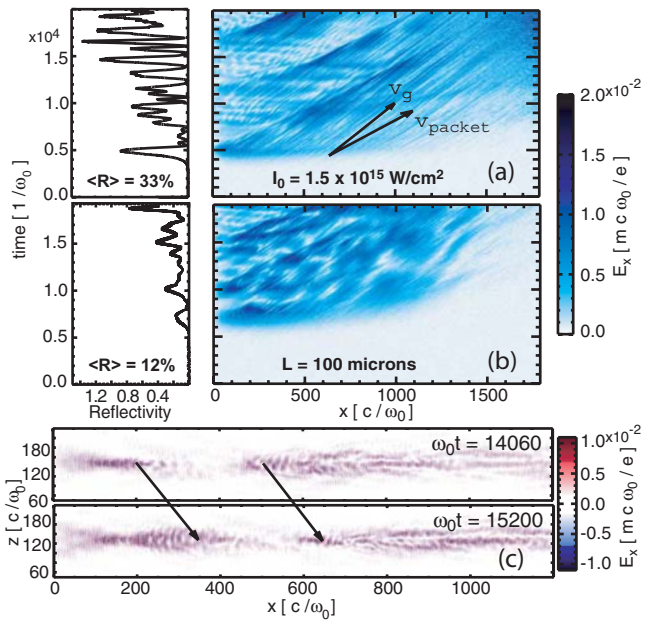


FIG. 3. (Color online) [(a) and (b)] Time vs reflectivity (left) and time vs space of the $E_x$ field (right) for (a) 1D and (b) 2D. The 1D simulation has $L=100$ $\mu$m and $I_0=1.5\times10^{15}$ W/cm$^2$. (c) $E_x$ field of the 2D simulation at two different times.

reflectivity burst at $\omega_0 t\simeq9000$. Whereas the second burst of new SRS for the shorter length in Fig. 1(a) came from the region left behind by the first packet, here the second burst comes from renewed SRS growth in the region into which the first packet travels, as seen in Figs. 2(a) and 2(b), left, where the second major burst in reflected light is generated deep into the plasma at $x\omega_0/c\simeq800$. As predicted for backscatter, the rear of the packet has the highest amplitude and furthermore continuously scatters light, thereby locally depleting the laser intensity. The whiter and bluer regions of Fig. 2(b), right, show how the depleted pump drives the plasma at a lower intensity than its incident intensity. As the initial packet's energy is etched away and the packet shrinks, it depletes less and less of the pump, as seen in the transmittivity. By $\omega_0 t=7500$, the full laser intensity passes the packet's rear edge, allowing it to penetrate deeper into the plasma and excite the packet more strongly. The process results in renewed packet growth and the large burst of reflectivity at $\omega_0 t=9000$.

Finally, the scattered light in the longer length plasma can come from SRS interactions between multiple packets, in contrast to the short systems in which only one packet is present at a time. These multipacket interactions steadily increase the amplitude of the reflectivity bursts in time. For instance, scattered light generated from the packet at $(x\omega_0/c,\omega_0 t)=(800,16\,000)$ can also interact with the packet at (400, 16 000) on its path to the rear edge. To illustrate, Fig. 2(c) shows the frequency content of the plasma and backscattered light waves late in time ($\omega_0 t=15\,000$ and 16 000) when there are two distinct packets in the simulation domain. The frequency plots are obtained by a fast Fourier transform (FFT) of the longitudinal and transverse $E$ fields, with a Gaussian-shaped window with FWHM$=832\omega_0^{-1}$ and size $\omega_0 t=2000$ centered about the time shown. At $\omega_0 t=15\,000$, the linear SRS frequencies of the backscattered light and plasma waves can be seen in the newly growing burst (packet 1 at $x\omega_0/c\simeq400$). In addition, the convecting packet (packet 2 at $x\omega_0/c\simeq800$) and its backscattered light can be seen at shifted frequencies. At $\omega_0 t=16\,000$, packet 1 has shifted down to a frequency which is resonant with the frequency up-shifted light traveling toward it from packet 2. The magnitude of packet 1 now increases, having shifted into a new resonance. As can be seen in Fig. 2(b), left, the scattered light from packet 2 also increases in amplitude as it passes through packet 1. The reflected and nonlinearly shifted light from packet 1 is then larger, which leads to larger bursts due to the nonresonant excitation of plasma waves described earlier. Specifically, the reflectivity bursts between $\omega_0 t=17\,000$ and 20 000 are larger than the bursts between 14 000 and 16 000, which are in turn larger than the bursts between 10 000 and 12 500.

All of the above effects contribute to the complex SRS behavior for higher dimensions as well. A comparison of results between 1D and 2D simulations is shown in Fig. 3, where both have a length of 100 $\mu$m (longer than that of Fig. 2) and the 1D laser intensity has been chosen to be the 2D laser intensity at the incident edge, $I_0=1.5\times10^{15}$ W/cm$^2$. Figure 3(a) shows 1D simulation results, while Fig. 3(b) shows 2D results. The reflectivity has been summed over the transverse dimension at the incident edge [Fig. 3(b), left], and the $E_x$ field is along the centerline of the domain [Fig. 3(b), right]. Figure 3(c) shows a zoomed-in region of the $E_x$ field at two times.

In the 1D case, the plasma waves and reflectivity evolve similarly as before, with packets that move at $v_{packet}$ and scatter light at a rate determined by the frequency shift. The first packet locally depletes the incident laser energy, but as trapped particles progressively etch it, the pump is more weakly depleted by $\omega_0 t = 8000$ and there is renewed packet growth, resulting in the larger reflectivity bursts at $\omega_0 t = 8000$. The reflectivity continues to grow in amplitude as time evolves. It is important to note that the increase is not due solely to scaling the shorter run's reflectivity up by the ratio of the box lengths. The longer box allows for packet interaction via scattered light traveling between packets and ultimately leads to higher reflectivity.

The total time-averaged reflectivity is lower for the 2D case (12%) versus the 1D, 100 $\mu$m case (33%). A focused Gaussian profile was used in the 2D case, so geometric effects related to varying laser intensity across the spot, the finite width of the plasma wave, and the finite spread in incoming angles all led to a decrease in overall reflectivity. Furthermore, nonlinear finite spot-size effects such as transverse localization of 2D plasma packets driven by SRS (see [9]) further reduce the SRS activity to the central axis after saturation. More details on the localization mechanisms will be left to a separate publication. Although localization occurs, it does not completely destroy the packets, as may be seen in Fig. 3(c). The filamentary structures consist of saturated, transversely localized plasma wave packets that convect through the simulation domain. Even though localization limits SRS activity off-axis and reduces reflectivity levels from 1D, the packets have roughly comparable peak amplitudes, implying that SRS is still 1D-like along axis.

Figure 3 also shows that packets affect SRS in 2D in a similar manner to 1D. First, the reflectivity has a periodicity that is determined by the recurrence of new bursts and a finer-scale recurrence from continued scattering off convecting packets that is determined by the nonlinear frequency shift. Second, the nonlinear packet velocity is approximately equal in both 1D and 2D simulations, implying that the etching rate that was theorized in Ref. [7] can be extended to higher dimensions, although Fig. 3(b), right, only shows the behavior of the plasma waves along the central axis and does not reveal the extent to which etching affects the packets off-axis. Finally, the reflectivity increases as a function of time, implying that scattered light interacts with multiple packets. Figure 3(c) shows how a newly saturated and localizing burst of plasma waves (on left) undergoes new growth and widens as it interacts with the backscattered light coming from the packet in front of it; the arrows show how far a point moving at the group velocity would travel.

In conclusion, we have shown how SRS behavior is affected by plasma wave packets. The nonlinear packet speed and the nonlinear frequency shift of plasma waves in the packet both determine a recurrence rate. In addition, packets locally deplete energy from the pump; as the packets are etched away and deplete less energy, the pump can then more fully penetrate the packet to drive renewed SRS growth. Finally, scattered light can travel between and interact with multiple packets, increasing the SRS reflectivity.

This work was supported by DOE under Grant Nos. DE-FG52-06NA26195, DE-FG52-09NA29552, and DE-FG02-03ER54721, by NSF under Grant Nos. NSF-Phy-0321345 and NSF-Phy-0904039, and by LLNL. Simulations were carried out on the UCLA DAWSON cluster.

[1] H. X. Vu, D. F. DuBois, and B. Bezzerides, Phys. Rev. Lett. **86**, 4306 (2001); Phys. Plasmas **9**, 1745 (2002).

[2] S. Brunner and E. J. Valeo, Phys. Rev. Lett. **93**, 145003 (2004).

[3] L. Yin *et al.*, Phys. Plasmas **13**, 072701 (2006).

[4] D. J. Strozzi, E. A. Williams, A. B. Langdon, and A. Bers, Phys. Plasmas **14**, 013104 (2007).

[5] M. Albrecht-Marc *et al.*, Phys. Plasmas **14**, 072704 (2007).

[6] H. X. Vu, D. F. DuBois, and B. Bezzerides, Phys. Plasmas **14**, 012702 (2007).

[7] J. E. Fahlen, B. J. Winjum, T. Grismayer, and W. B. Mori, Phys. Rev. Lett. **102**, 245002 (2009).

[8] R. G. Hemker, Ph.D. thesis, University of California, Los Angeles, 2000; R. A. Fonseca *et al.*, Lect. Notes Comput. Sci. **2331**, 342 (2002); R. A. Fonseca *et al.*, Plasma Phys. Controlled Fusion **50**, 124034 (2008).

[9] L. Yin, B. J. Albright, K. J. Bowers, W. Daughton, and H. A. Rose, Phys. Rev. Lett. **99**, 265004 (2007); Phys. Plasmas **15**, 013109 (2008).

[10] G. J. Morales and T. M. O'Neil, Phys. Rev. Lett. **28**, 417 (1972).

[11] D. Bénisti and L. Gremillet, Phys. Plasmas **14**, 042304 (2007); D. Bénisti, D. J. Strozzi, and L. Gremillet, *ibid.* **15**, 030701 (2008).

[12] R. R. Lindberg, A. E. Charman, and J. S. Wurtele, Phys. Plasmas **14**, 122103 (2007).

[13] B. J. Winjum, J. Fahlen, and W. B. Mori, Phys. Plasmas **14**, 102104 (2007).

[14] T. P. Coffey, Phys. Fluids **14**, 1402 (1971).